

QUASI-PERIODIC PULSE AMPLITUDE MODULATION IN THE ACCRETING MILLISECOND PULSAR IGR J00291+5934

PETER BULT,¹ MARIEKE VAN DOESBURGH,² AND MICHEL VAN DER KLIS²

¹*Astrophysics Science Division, NASA Goddard Space Flight Center, Greenbelt, MD 20771, USA*

²*Anton Pannekoek Institute, University of Amsterdam, Postbus 94249, 1090 GE Amsterdam, The Netherlands*

ABSTRACT

We introduce a new method for analysing the aperiodic variability of coherent pulsations in accreting millisecond X-ray pulsars. Our method involves applying a complex frequency correction to the time-domain light curve, allowing for the aperiodic modulation of the pulse amplitude to be robustly extracted in the frequency domain. We discuss the statistical properties of the resulting modulation spectrum and show how it can be correlated with the non-pulsed emission to determine if the periodic and aperiodic variability are coupled processes. Using this method, we study the 598.88 Hz coherent pulsations of the accreting millisecond X-ray pulsar IGR J00291+5934 as observed with the *Rossi X-ray Timing Explorer* and *XMM-Newton*. We demonstrate that our method easily confirms the known coupling between the pulsations and a strong 8 mHz QPO in *XMM-Newton* observations. Applying our method to the *RXTE* observations, we further show, for the first time, that the much weaker 20 mHz QPO and its harmonic are also coupled to the pulsations. We discuss the implications of this coupling and indicate how it may be used to extract new information on the underlying accretion process.

Keywords: pulsars: general – stars: neutron – X-rays: binaries – X-rays: individual (IGR J00291+5934)

1. INTRODUCTION

Accreting millisecond X-ray pulsars (AMXPs) are a subclass of transient low-mass X-ray binaries (LMXBs) for which the stellar rotation rate of the central neutron star is directly apparent in the form of coherent pulsation. Such pulsations manifest as nearly sinusoidal oscillations in the X-ray flux with fractional sinusoidal amplitudes of a few to about ten percent (Patruno & Watts 2012).

Pulsations are thought to be due to magnetically channeled accretion, such that the impact of the accretion column gives rise to local emission regions, hotspots, near the stellar magnetic poles. Due to the stellar rotation such hotspots undergo periodic aspect variations, which leads to the observed flux variations.

The accretion flow powering coherent pulsations is variable in its own right. Like the wider class of LMXBs, AMXPs show aperiodic X-ray variability over a wide range of timescales, including broad band-limited noise structures and narrow quasi-periodic oscillations (QPOs). These aperiodic features have a rich structure of trends and relations (van Straaten et al. 2005) that is nearly identical to the variability observed in non-pulsating accreting neutron stars (van der Klis 2006).

Because the pulsations are powered by the accretion flow, it may be expected that the periodic emission is coupled to the aperiodic variability. Considering the coherent and aperiodic variability together gives a potential diagnostic of accretion physics. Measuring the degree of coupling, and exploring its dependence on energy or luminosity, can give additional constraints on the physical models aiming to explain quasi-periodic variability, the magnetic coupling of the neutron star and the accretion flow, and the emission pattern of the hotspot on the stellar surface. Lacking a robust method for analysing such coupling, however, previous studies have relied on ad-hoc or model-dependent approaches.

Analysing observations of the canonical accreting millisecond pulsar SAX J1808.4–3658, Menna et al. (2003) assume that the band-limited noise is produced by a shot noise process and derive an analytic model power spectrum for the scenario where the shot noise emission originates partially from the neutron star hotspot. This model could be successfully fit to observations, which suggests that the periodic and aperiodic components indeed show coupled behavior, but its results are otherwise difficult to interpret. This approach is complicated further by the reliance on a shot noise model, which is ruled

out by the flux-dependent amplitudes that are observed in both the periodic and aperiodic components of SAX J1808.4–3658 (Uttley & McHardy 2001; Uttley 2004).

Considering the relation between an aperiodic flaring component and the coherent pulsations in SAX J1808.4–3658, Bult & van der Klis (2014) selected the flares in the time domain and calculated the pulse properties as a function of flux. While model independent, this approach only works in rare cases where the aperiodic signal is directly visible in the light curve.

In a similar example, Ferrigno et al. (2017) measured pulse properties over short time segments. Rather than using the flux distribution, they computed the power spectrum for a series of consecutive pulse amplitude measurements. While this approach no longer requires the aperiodic variability to be directly resolved in the time domain, it does impose a minimum segment length in order to measure the pulse properties through epoch folding. Hence, only aperiodic features that vary on timescales that are slower than the folding segment length can be studied in this way. Furthermore, this approach is difficult to interpret as well, as the statistical properties of such a power spectrum are not obvious.

In this work we consider the problem of analysing the coupling between the periodic and aperiodic variability of AMXPs, and propose a method targeted specifically at quantifying such coupling. In section 2 we describe our analysis method in detail, and in sections 4 and 5 we demonstrate its use by applying it to observations of the accreting millisecond pulsar IGR J00291+5943.

1.1. IGR J00291+5934

The transient X-ray binary IGR J00291+5934 (IGR J00291) is a 598.88 Hz accreting millisecond pulsar in a 2.45 hour binary (Markwardt et al. 2004) located at a distance of 4.2 ± 0.5 kpc (De Falco et al. 2017). This pulsar was discovered with *INTEGRAL* in December 2004 (Eckert et al. 2004; Shaw et al. 2005), when it showed an outburst lasting approximately 15 days. In August and September 2008 the source was again detected, showing two separate outbursts each peaking at a flux level half that observed in 2004 (Chakrabarty et al. 2008; Lewis et al. 2008). The next major outburst, in July 2015, more closely resembled the behavior observed in 2004 (De Falco et al. 2017; Sanna et al. 2017).

The pulse profiles of IGR J00291 are nearly sinusoidal, with typical sinusoidal fractional amplitudes of 8 – 12% for the fundamental and $\sim 0.5\%$ or less for the second harmonic (Galloway et al. 2005; Falanga et al. 2005). Tracking the arrival times of the pulsations showed that the pulse frequency increases while the source is actively accreting and decreases when it is not (Patruno 2010; Papitto et al. 2011), which is interpreted as evidence for the accretion torque spinning up the neutron star during outburst, and magnetic dipole radiation causing a spin-down during quiescence. The pulse phase was also observed to change linearly with X-ray flux (Patruno

2010), likely indicating that the neutron star hotspot moves over the stellar surface as the mass accretion rate changes (Patruno et al. 2009).

The aperiodic variability of IGR J00291 is somewhat anomalous as compared to other AMXPs (Linares et al. 2007; Hartman et al. 2011). In both the 2004 and 2008 outbursts the power spectrum could be adequately described with 3 to 4 broad noise components, together covering the 0.01–100 Hz range. The power spectral shape resembles that of a typical atoll extreme island state (see, e.g. van Doesburgh & van der Klis 2017 for a recent overview of the atoll states and their power spectra), but has a much larger than usual total fractional variability of $\sim 50\%$ rms and lower than typical characteristic frequencies ranging from about 0.04 Hz up to 70 Hz. Additionally, two harmonically related QPOs are observed at ~ 20 mHz and ~ 40 mHz that appear more like the low-frequency QPOs observed in black holes (Linares et al. 2007) than any feature normally seen in accreting neutron stars. The 2015 outburst showed a similar band-limited noise structure, but different QPOs (Ferrigno et al. 2017). In that outburst a prominent 8 mHz QPO was observed at low (< 2 keV) energies.

Our choice for IGR J00291 as a test case is motivated by its high pulse frequency and relatively large pulse fraction. The combination of a high pulse frequency and lack of fast (> 100 Hz) QPOs ensures that there is little contaminating variability around the pulse frequency in the Fourier domain, while a large pulse fraction naturally contributes to a better significance in measuring the coupling.

2. ANALYSIS METHOD

In this work we consider a simple premise: if the neutron star surface emission (i.e. the hotspot) couples to the variable accretion flow, then the pulse amplitude should, to some degree, exhibit the same aperiodic periodicities as that flow. Our aim, then, is two-fold; first we want to define a Fourier transform of the pulsed emission to establish if the pulsations indeed show an aperiodically variable amplitude. If confirmed, the second step is to analyse if and how that aperiodicity correlates with the Fourier transform of the non-pulsed flux.

2.1. Pulse modulation spectrum

We define the pulse signal at time t as

$$x(t) = a_0(t) + a_1(t) \cos(2\pi\nu_p t + \varphi_p), \quad (1)$$

where ν_p is the pulse frequency, and φ_p its phase offset. The function $a_0(t)$ gives the aperiodic non-pulsed emission, and $a_1(t)$ is the *instantaneous amplitude*, which is further specified as

$$a_1(t) = m_0 + m(t). \quad (2)$$

Here m_0 gives the averaged pulse amplitude as measured by the usual coherent timing analyses (see, e.g. Hartman

et al. 2008), and $m(t)$ is a generic zero-mean modulation function describing the stochastic variations about the mean amplitude. Our goal is to obtain the Fourier transform of $m(t)$.

The last term in our expression for the pulse signal (eq. 1) is equivalent to an amplitude modulated (AM) carrier wave. The Fourier convolution theorem (Bracewell 1965) then implies that the spectrum of $m(t)$ appears in the Fourier transform of $x(t)$ as sidebands around the carrier frequency ν_p . This spectral information can be extracted if we *demodulate* the light curve, which amounts to applying a frequency shift in the Fourier domain. Applying the Fourier shift theorem (Bracewell 1965), we write the demodulated light curve as

$$z(t) = x(t)e^{-2\pi i\nu_p t - i\varphi_p}, \quad (3)$$

so that the Fourier transform at frequency f is given as

$$\begin{aligned} Z(f) &= \int_{-\infty}^{\infty} z(t)e^{-2\pi i f t} dt, \\ &= A_0(f + \nu_p)e^{-i\varphi_p} + \frac{1}{2} [m_0\delta(f) + M(f)] \\ &\quad + \frac{1}{2} [m_0\delta(f + 2\nu_p) + M(f + 2\nu_p)]e^{-i2\varphi_p}, \quad (4) \end{aligned}$$

where $\delta(f)$ gives the Dirac delta function and upper case letters are used to indicate the Fourier transforms of lower case time domain functions. We see that modulation spectrum, $M(f)$, makes two contributions; once centered at zero frequency and once centered at $-2\nu_p$. These two contributions have an Hermitian symmetry¹, about frequency $-\nu_p$ so we can capture all information with only one of these two contributions. The spectrum of the non-pulsed emission, $A_0(f)$, acts as a contaminating background term. If this spectrum is band-limited to cut off well below the pulse frequency, then we can effectively separate all terms in frequency space, and write

$$Z(f) = \frac{1}{2} M(f), \quad (5)$$

for $0 < |f| \ll \nu_p$. This is a fair assumption for IGR J00291, but does not hold in general. We therefore caution that for AMXPs that show aperiodic variability at frequencies comparable to ν_p there may be some contamination in eq. 5 from the high-frequency tails of $A_0(f)$ that should be accounted for.

The pulse modulation spectrum, $M(f)$, is not necessarily symmetrical around zero frequency. Depending on how, exactly, the periodic emission is modulated, this spectrum may show features at negative frequencies, at positive frequencies, or both. For instance, the beat frequency between two azimuthal rotations would cause a

¹ Hermitian symmetric functions have the symmetry relation $H(f) = H^*(-f)$, where $*$ denotes the complex conjugate. In our case the symmetry is about $f = -\nu_p$ rather than $f = 0$ due to the applied frequency shift operation.

strictly one-sided modulation spectrum, whereas a surface temperature oscillation could cause a symmetrical modulation spectrum. To proceed, we therefore extract separate modulation sidebands for both the positive or negative frequencies.

A known difficulty in the analysis of pulse sidebands is that observations are discretely sampled, so that windowing and spectral leakage cause spurious broadening of the pulse spike (Lazzati & Stella 1997; Burderi et al. 1997). Both phenomena can be described at once by considering that the Discrete-Time Fourier Transform (DTFT) can be written as a convolution (Bloomfield 1976)

$$\begin{aligned} \tilde{X}(f) &= \sum_{j=0}^{N-1} x(j\Delta t)e^{-2\pi i j \Delta t f}, \\ &= X(f) \otimes D_N(f), \quad (6) \end{aligned}$$

where we use \otimes to indicate the convolution. The light curve is measured at N discrete intervals with time resolution Δt and

$$D_N(f) = \frac{\sin(\pi f / \Delta f)}{\sin(\pi f / N \Delta f)} e^{i(N-1)\pi f / N \Delta f} \quad (7)$$

is a version of the Dirichlet kernel (Titchmarsh 1939). We also used $\Delta f = 1/N\Delta t$ so that the more familiar Discrete Fourier Transform (DFT) is obtained by evaluating eq. 6 only at the discrete Fourier frequencies $k\Delta f$, where $k = -N/2, \dots, 0, \dots, N/2 - 1$. For a complex waveform $x_j = e^{2\pi i j \kappa / N}$ with frequency $f_{\text{wave}} = \kappa\Delta f$, we get the DTFT

$$\tilde{X}_{\text{wave}}(f) = D_N((k - \kappa)\Delta f), \quad (8)$$

which we show in Figure 1 for two values of κ . It can be seen that the wave frequency parameter κ acts to translate the response of the Dirichlet kernel. The observed spectral leakage in the DFT then arises if κ is not an integer. Notice, however, that the demodulation of the light curve (eq. 3) acts to precisely align the Fourier transform with the pulse frequency. The Fourier frequency samples then coincide with the zero crossings of the Dirichlet kernel, ensuring that the pulse spike will not be broadened outside the zero frequency bin of the DFT.

An additional distortion comes from the fact that the discrete measurements reflect an integration over the width of a time bin rather than an instantaneous sample as assumed above. This effect can be described by convolving the time domain function with a binning window (van der Klis 1989). In the frequency domain this distortion causes slightly suppressed amplitudes, but it will not bias the phases. Additionally, if the amplitude of the coherent wave is modulated, then the modulation spectrum itself will still suffer from sampling effects, however, those effects will be identical to the ones

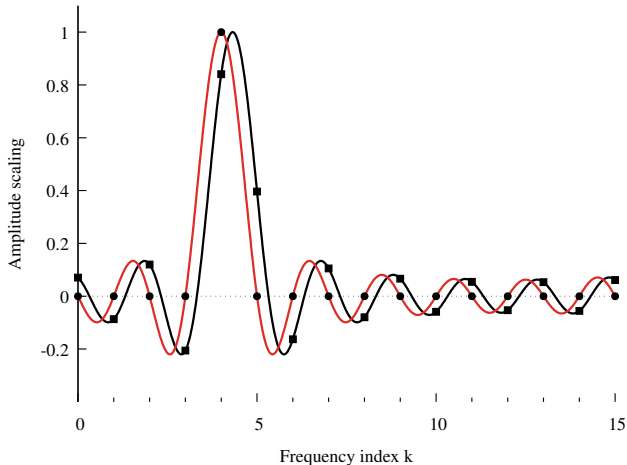


Figure 1. Discrete-Time Fourier Transform of a complex wave for $N = 16$ and $\kappa = 4$ (red, circles) and $\kappa = 4.32$ (black, squares). The curves show the Dirichlet kernel response and the symbols mark the samples of the usual Discrete Fourier Transform (DFT). Note that for $\kappa = 4$ the DFT samples coincide with the kernel zero-crossings, thus minimizing spectral leakage.

affecting the low frequency range of the regular power density spectrum.

Writing the discrete version of the modulation spectrum

$$M_k = \begin{cases} 2Z_k, & \text{positive frequency sideband,} \\ 2Z_{-k}^*, & \text{negative frequency sideband,} \end{cases} \quad (9)$$

we obtain the Leahy-normalized modulation power spectrum (Leahy et al. 1983) as

$$P_{k,\text{Leahy}} = \frac{1}{2N_\gamma} |M_k|^2, \quad (10)$$

where N_γ gives the number of photons in the time series. For counting noise data the resulting powers are χ^2 distributed for 2 degrees of freedom, and can be treated on the same footing as the regular power density spectrum (see, e.g, van der Klis 1989).

While the Leahy(-like) normalization is useful to determine the uncertainties on the computed powers, it is more informative to consider the rms normalization. We express the powers in units of rms as a fraction of the mean pulse amplitude, rather the mean intensity. The squared fractional rms normalization can be obtained by scaling the Leahy(-like) powers as

$$P_{k,\text{rms}} = \frac{4}{a^2} \frac{T}{N_\gamma} P_k, \quad (11)$$

where $T = N\Delta t$ gives the duration of the time series, $a = m_0/\langle a_0 \rangle$ is the fractional sinusoidal amplitude of the pulsation, with $\langle a_0 \rangle$ the time average of $a_0(t)$.

If we find that the two sidebands produce statistically consistent power spectra, and that they form a complex conjugate pair in the complex plane, then we have demonstrated the modulation spectrum is Hermitian about zero frequency. This immediately puts a constraint on which physical processes might cause the modulation. Additionally, we can exploit this symmetry by treating each of the two sidebands as independent samples of the same underlying spectrum. This allows us to improve the statistical quality of the modulation spectrum by averaging the sidebands in the complex plane before computing the modulation power density spectrum.

2.2. The modulation coherence

If the stochastic variation of the pulse amplitude, $m(t)$, is coupled to aperiodic variability, then the non-pulsed emission term $a_0(t)$ should also have some dependence on that modulation. In the Fourier domain this results in a phase relation between $M(f)$ and the low frequency part of the normal spectrum, $A(f)$, that can be studied using the cross-spectrum (Jenkins & Watts 1968).

Exactly how the modulation term enters into the non-pulsed emission depends on the assumed accretion geometry and the various origins of the emission components. For instance, one may assume that a part of the hotspot is always in the observer's line-of-sight, so that $m(t)$ contributes directly to $a_0(t)$. Through emission from the accretion disk, we may also be able to observe the modulation term directly, possibly at a time-lag with respect to the pulse modulation. Additionally, either of these two contributions may be non-linear.

In this work, however, we take a first order approach and consider the direct Fourier transform of the light curve, $X(f)$, as an estimator of $A(f)$ and proceed to analyse its linear correlation with $M(f)$. Hence, we define the complex-valued cross spectrum

$$C(f) = X(f)M^*(f), \quad (12)$$

where $M(f)$ is given by eq. 9. Casting the cross spectrum in complex polar form, we can extract the co-amplitude spectrum by taking the absolute value of $C(f)$. To measure the degree of coupling it is more convenient to normalize the co-amplitudes to a coherence measure (Vaughan & Nowak 1997)

$$|\gamma|^2 = \frac{|\langle C \rangle|^2 - n^2}{\langle P_X \rangle \langle P_M \rangle}, \quad (13)$$

where

$$n^2 = \frac{1}{K} \left\{ \langle P_X \rangle P_{\text{noise},M} + \langle P_M \rangle P_{\text{noise},X} - P_{\text{noise},X} P_{\text{noise},M} \right\} \quad (14)$$

corrects for the bias due to the presence of Poisson counting noise power, P_{noise} , and $\langle \cdot \rangle$ represents an ensemble average over K independent light curve segments and/or adjacent frequency bins. Finally we can consider the phase of the cross spectrum, $\phi(f)$, to establish whether the pulse modulation is leading or lagging behind $X(f)$.

3. DATA REDUCTION

We analyse observations of all observed outbursts of IGR J00291. For the 2015 outburst we consider an *XMM-Newton* observation. For the outbursts of 2008 and 2004 we consider observations with the *Rossi X-ray Timing Explorer (RXTE)*.

3.1. *XMM Newton*

The 2015 outburst of IGR J00291 was observed with *XMM-Newton* on July 28 (ObsID 0744840201). We analyse the EPIC-PN data, which was collected in TIMING mode, providing event data at a time resolution of 29.56 μs .

We process the *XMM-Newton* data with SAS version 15.0.0, using the most recent calibration files available. Standard screening criteria were applied, selecting only those events in the energy range 0.4 – 10 keV with PATTERN ≤ 4 and screening FLAG = 0. The source events were extracted from the RAWX coordinates [34 : 43]. Likewise, the background count rate was extracted from the [3 : 5] range.

The extracted event arrival times were corrected to the Solar System barycenter using the BARYCEN tool, based on the source coordinates of the optical counterpart (Torres et al. 2008). Subsequently the arrival times were adjusted for the binary motion of the neutron star based on the ephemeris of Sanna et al. (2017).

3.2. *RXTE*

We analyze all pointed *RXTE* observations of the 2008 (Proposal number 93013 / 93435) and the 2004 (Proposal number 90052 / 90425) outbursts of IGR J00291. We consider all GoodXenon and (122 μs) Event data, applying standard screening criteria (source elevation above 10° and pointing offset less than 0.02°) and selecting only those events in energy channels 5 to 48 ($\sim 2\text{--}20$ keV).

Using the source coordinates of Torres et al. (2008) we correct the photon arrival times to the Solar System barycenter using the FTOOL FAXBARY, which also applied the *RXTE* fine clock corrections. We then use the binary ephemeris reported by Patruno (2010) to correct the data for the binary motion of the neutron star.

The *RXTE* data is contaminated by the foreground emission of the nearby Intermediate Polar V709 Cas (Falanga et al. 2005). Because this source does not contribute to the variability above 5 mHz (Linares et al. 2007) we can treat it as an additional contribution to

the background emission. We use the FTOOL PCABACKEST to estimate the instrumental background level and correct for estimated count rate of V709 Cas (Linares et al. 2007; Hartman et al. 2011).

3.3. *Timing*

For both the *RXTE* and *XMM-Newton* observations we bin the data to a time resolution of $\sim 240 \mu\text{s}$ and divide the light curves into segments of ~ 1000 s. Fourier transforms of these light curve segments then have a frequency resolution of ~ 1 mHz and a limiting Nyquist frequency of ~ 2000 Hz.

To construct the pulse amplitude modulation power spectra we first fold each data segment on the pulse period and measure the local pulse phase and amplitude. We then demodulate the time series using eq. 3 and use eq. 10 to construct the power spectra. For the *XMM-Newton* data we average all spectra in the ObsID, while for the *RXTE* observations we use the data grouping of Linares et al. (2007) and Hartman et al. (2011).

Because the shifting operation of eq. 3 will affect the dead time process in a non-trivial way, the Poisson noise model of Zhang et al. (1995) may not be appropriate. However, given that the considered count-rates are relatively low, dead time effects should be weak so that the Poisson noise power is well approximated by a constant. Following the approach of Klein-Wolt et al. (2004), we therefore fit a constant to the average power at high frequencies, which we then adopt as the Poisson noise level.

The Poisson noise-corrected spectra are renormalized to fractional rms with respect to the pulse amplitude (eq. 11) and fitted with a multi-Lorentzian model (Belloni et al. 2002), where each Lorentzian, $L(\nu; r, Q, \nu_{\text{max}})$, is expressed in terms of its integrated rms amplitude r , where

$$r^2 = P = \int_0^\infty L(\nu) d\nu, \quad (15)$$

its characteristic frequency ν_{max} , and quality factor Q . A component is accepted as significant if its integrated power, P , has a single-trial signal to noise ratio greater than three; that is, when $P/\sigma_P \geq 3$.

4. RESULTS

In the following we apply the methods discussed in section 2 to the observations of IGR J00291. We first present the results from the *XMM-Newton* data. This data contains a strong 8 mHz QPO that was previously shown to couple to the pulsations in a heuristic analysis (Ferrigno et al. 2017), and hence provides an opportunity to validate our method. Next we present the results from the *RXTE* data, for which low frequency QPOs have been reported (Linares et al. 2007; Hartman et al. 2011). These weak features may not be resolved directly in the light curve, and require a method as developed here to establish whether they too couple to the pulsed emission.

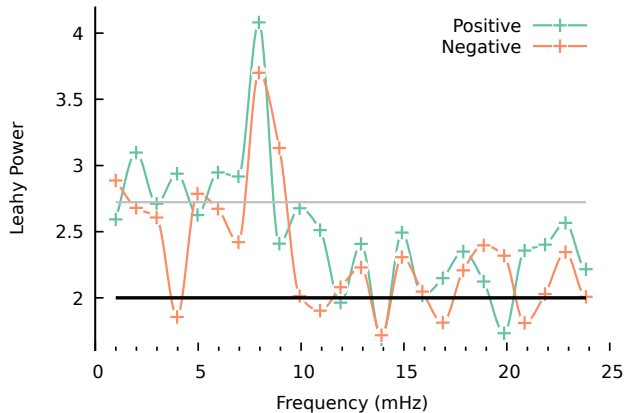


Figure 2. Pulse modulation power spectra of the *XMM-Newton* observation, showing both the positive and negative frequency sidebands. The black line indicates the Poisson noise power level and the grey line show the 3σ detection threshold.

4.1. *XMM-Newton*

To confirm that the 8 mHz QPO is coupled to the pulsed emission, we first calculate the modulation power spectrum for the positive and negative frequency sidebands of the pulsations. The lowest frequency samples of these spectra are shown in Figure 2. Both sidebands have a significant feature at 8 mHz. The sidebands are statistically consistent with each other, suggesting they are the symmetric wings of a single modulating function. If so, then the negative sideband should be the complex conjugate of the positive sideband (section 2.1). We can test this relation by measuring the complex phase angle at 8 mHz in each sideband, and then exploring the distribution of their sum. If the two features form a conjugate pair, then the summed phase should have, on average, zero phase. This phase distribution (shown in Figure 3) indeed has a preferential direction that is statistically consistent with being zero to within 20% uncertainty ($\phi = 0.1 \pm 1.4$), confirming that there is a single modulation mechanism that is responsible for both sidebands.

We proceed to construct the averaged-sideband pulse amplitude modulation power spectrum. That is, for each segment we extract the modulation spectrum by averaging the two sidebands in the complex plane. This averaged-sideband spectrum (Figure 4) shows a narrow QPO at 8 mHz with a fractional amplitude of 12% rms with respect to the mean pulse amplitude. The QPO is superimposed on a broad band-limited noise term with a characteristic frequency of 0.020 Hz, and a second noise term is found centered at 1 Hz. The detailed fit parameters are given in Table 1.

To explore the energy dependence of the QPO, we construct the modulation power spectrum for different energy bands. As shown in Figure 5 the fractional am-

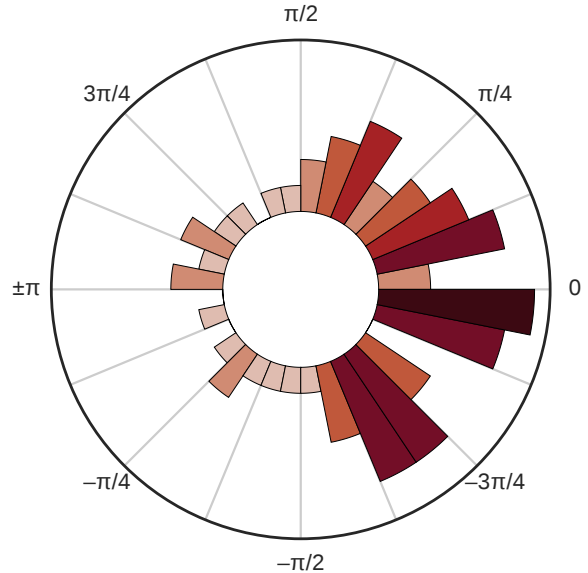


Figure 3. Histogram of the phase difference between the positive sideband modulation and the complex conjugate of the negative sideband modulation in the *XMM-Newton* observation, when both sidebands are evaluated at 8 mHz. The colors scale with the probability density such that darker colors phase bins indicate a larger number of occurrences in that direction. The average phase is consistent with zero ($\phi = 0.1 \pm 1.4$), indicating the two sidebands are symmetric.

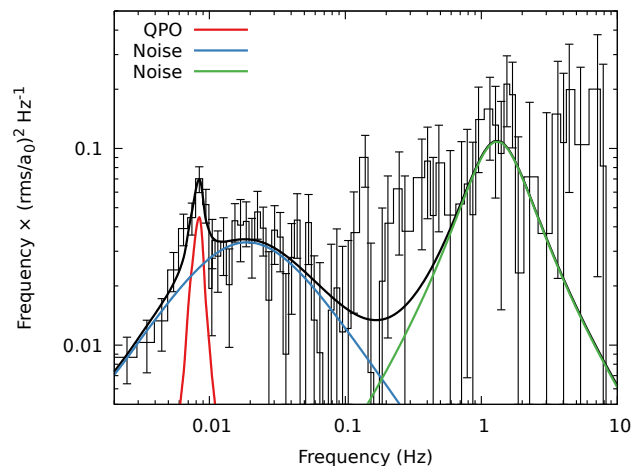


Figure 4. Pulse modulation power spectra in the 0.4 – 2 keV energy band of the *XMM-Newton* observation computed by averaging the positive and negative sideband. The curves give the best-fit model reported in Table 1.

plitude of the QPO peaks at 1 keV and drops rapidly with increasing energy. Above 4 keV the QPO could no longer be resolved in the modulation power spectrum. For comparison we have also measured the fractional

Table 1. Pulse amplitude modulation power spectrum fit results

Group	Component	Frequency (Hz)	Quality	Amplitude (% rms)	χ^2 / dof
2015					
	QPO	0.0082(2)	5(2)	12.1(1.8)	
XMM	noise ₁	0.019(3)	0 (fixed)	32.4(1.5)	74 / 75
	noise ₂	1.3(3)	0.7(4)	41(6)	
2004					
	break	0.36(13)	0 (fixed)	28.7(3.0)	
A1	QPO ₁	0.0195(14)	1.7(6)	11.7(1.4)	60 / 63
	QPO ₂	0.0445(16)	3.7(1.9)	10.8(1.8)	
A2	break	0.9(5)	0 (fixed)	46.1(7.6)	53/59
	noise	0.030(7)	0.20(18)	32.3(3.1)	
B	noise	0.031(9)	0.2(3)	60.7(6.7)	44/52
2008					
P1	noise	0.024(4)	0 (fixed)	92.3(58)	37 / 41
P2	noise	0.067(18)	0 (fixed)	95.8(90)	60 / 62

amplitude of the direct 8 mHz QPO and its harmonic component as observed in the regular power spectrum using the same energy bands. We find that both the direct 8 mHz QPO and the pulse amplitude modulation QPO show roughly the same energy dependence, and that the pulse modulation has a systematically lower fractional amplitude. Remarkably, the harmonic of the 8 mHz QPO as detected in the direct power spectrum has an opposite trend, showing an increasing amplitude for higher energy. Additionally, this harmonic is only detected in the direct power spectrum, and not in modulation power spectrum.

In order to conclusively prove that the 8 mHz QPO indeed couples to the pulsed emission, we compute the modulation coherence spectrum (eq 13) for the *XMM-Newton* observation, which we show in Figure 6. The spectrum shows a clear peak at 8 mHz, where the magnitude-squared coherence measure is ~ 0.5 . Considering the phase distribution of the cross spectrum, we find that the associated phase-lag at 8 mHz is consistent with being zero to within a 10% uncertainty, indicating the 8 mHz QPO in the pulse modulation is in phase with the corresponding feature in the direct power spectrum. The coherence spectrum shows additional peaks at 16 mHz and 24 mHz, each marginally detected with 3σ significances and having progressively smaller coherence measures. For these higher harmonics, however, the cross spectral amplitudes are too low to reliably measure the phase lag. If we construct the modulation coherence spectrum for higher energies, we find that, consistent with the direct power spectrum, the

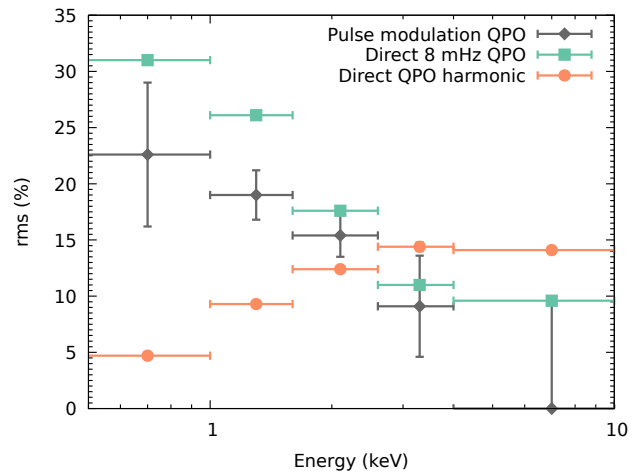


Figure 5. Fractional amplitude of the 8 mHz QPO as a function of energy, showing the QPO as measured in the regular power spectrum (green squares), and as measured in the modulation power spectrum (grey diamonds). Also shown is the amplitude of the QPO harmonic (orange circles) as detected in the regular power spectrum. The pulse modulation QPO is measured in terms of fractional rms with respect to the pulse amplitude, whereas the direct QPO and its harmonic are expressed in terms of fractional rms with respect to the mean flux.

8 mHz features becomes less pronounced. Meanwhile the coherence measure at the harmonic frequencies in-

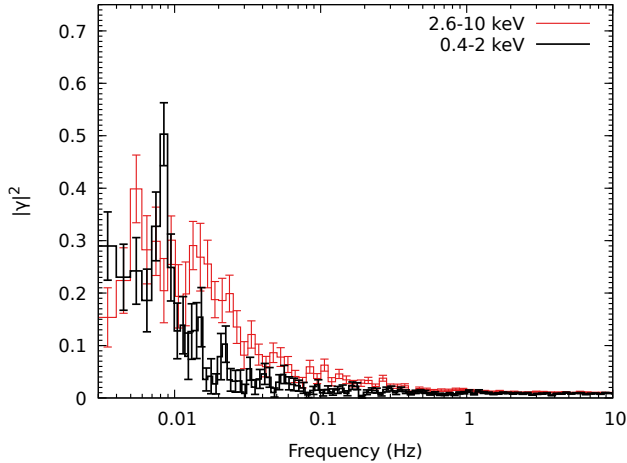


Figure 6. Pulse amplitude coherence spectrum in the 0.4 – 2 keV (black) and 2.6 – 10 keV (red) bands of the *XMM-Newton* observation.

creases, even though the peaks themselves can longer be individually resolved.

4.2. *RXTE*

Following the nomenclature of Linares et al. (2007), the *RXTE* observations of the 2004 outburst are divided into three groups; set A1, set A2, and set B. For each set we calculate the modulation power spectrum, using a bandwidth of 200 Hz. The spectra show no features above 10 Hz, so we use the 20 Hz to 200 Hz range to compute the Poisson noise level and subsequently truncate the spectra above 10 Hz before proceeding with the multi-Lorentzian fit.

Following the same procedure as in the previous section, we first construct the pulse amplitude modulation power spectra for the positive and negative sidebands of the pulse spike separately. We find that both spectra show a broad noise structure at mHz frequencies, with individual peaks on top of them. With a significance of $\sim 2\sigma$, these peaks are not formally detections, however, they have coincident frequencies between the two sideband spectra.

If the two sidebands represent the same underlying spectrum, then using the averaged sideband should boost the signal-to-noise of these features. We therefore proceed by constructing the modulation power spectra for the averaged sideband, in which we indeed detect statistically significant QPOs. The spectrum is shown in the top panel of Figure 7, and can be described with two QPOs at characteristic frequencies of 20 mHz and 44 mHz, and an additional broad noise component with a characteristic frequency of 0.4 Hz (see Table 1 for details). These QPOs are consistent with those reported by Linares et al. (2007) for the direct power spectrum, although the fractional amplitude of the modulation QPOs is twice that of the direct QPOs.

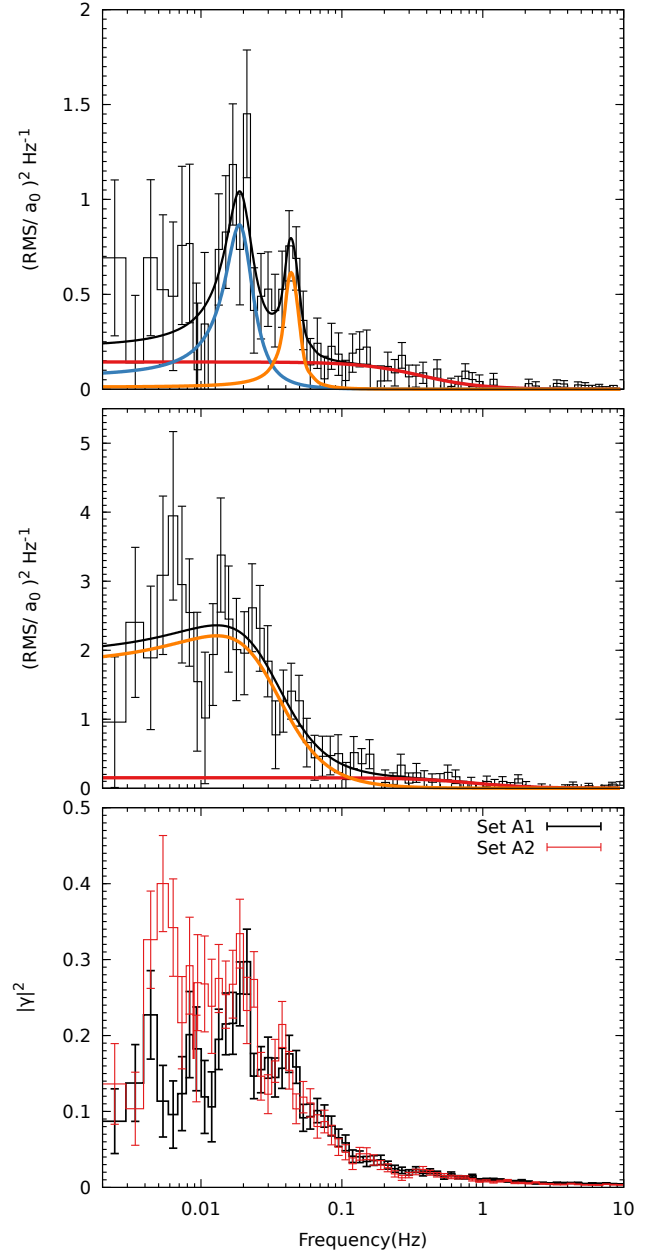


Figure 7. Pulse amplitude modulation power spectra for set A1 (top panel) and A2 (middle panel) of the 2004 outburst with their best fit multi-Lorentzian models, and the modulation coherence spectra of both sets (bottom panel). See Table 1 for the model fit parameters.

For set A2 we again find that a broad noise component is present in the positive and negative sidebands of the pulse spike, and construct the pulse amplitude modulation spectrum for the averaged sideband. The resulting spectrum again shows features at 20 and 44 mHz, however, they could not be individually resolved. Instead we describe the power in that frequency range using a single broad noise component (see Figure 7 middle panel).

The spectrum also shows an additional excess of power at a frequency of 6 mHz, however, with a 2σ detection level this feature is not statistically significant.

Finally, set B covers the tail of the outburst, where both the source count rate and the pulse fraction have decreased (see Mukherjee et al. (2015) for the pulse fraction as a function of time). Because the signal-to-noise is much lower, we had to smooth the spectra over wide frequency bins to be able to detect the power. A single broad noise component provided an adequate fit to the averaged sideband modulation power spectrum. This noise term has a similar shape and frequency as the mHz noise term seen in set A2, but shows a higher fractional rms.

Following section 2.2, we also calculated the modulation coherence spectra for the three sets. The coherence spectra of all sets show a broad structure below 0.1 Hz, and for sets A1 and A2 a number of peaks are observed (see Figure 7). For set B the required smoothing prohibited the detection of such narrow features. In the case of set A1 there are distinct peaks in the coherence measure at roughly 20, 40 and 60 mHz, indicating that mHz QPOs are coupled to the pulsations. The modulation coherence spectrum of set A2 shows similar peaks, suggesting the presence of a coupled component despite the modulation power spectrum being poorly resolved. Additionally, a prominent peak exists in the modulation coherence spectrum at 6 mHz, which would suggest that the power excess at 6 mHz that was seen in the modulation power spectrum is a real component.

Following the analysis of Hartman et al. (2011), we group the *RXTE* observations of the 2008 outbursts in two sets; one for each partial outburst, and perform the same analysis. The modulation power spectra of these two outbursts are very similar (see Table 1 for the fit parameters). Although a number of very narrow features may be seen in the spectra, none are statistically significant. Instead both spectra are adequately described with just a single broad noise component. Those noise terms, however, do have a remarkably large amplitudes, showing fractional amplitudes in excess of 90% rms with respect to the pulse amplitude. The modulation coherence spectra show a broad structure as well, with a magnitude squared coherence measure of ~ 0.25 below 30 mHz, and no resolved peaks.

5. DISCUSSION

Using specialized methods introduced in this work, we have analysed the coupling of the millihertz QPOs in IGR J00291 with its 599 Hz pulsations. We can distinguish two instances of mHz QPOs, namely the 8 mHz QPO observed with *XMM-Newton* in the 2015 outburst (Ferrigno et al. 2017) and the ~ 20 mHz and its harmonics as seen in *RXTE* observations of earlier outbursts (Linares et al. 2007; Hartman et al. 2011). Because the two versions of millihertz variability are not observed simultaneously, nor in the same energy band, it is unclear

if they share the same underlying physical mechanism (Ferrigno et al. 2017). In the following we therefore first discuss the *XMM-Newton* and *RXTE* results separately, before briefly considering them together.

5.1. The 8 mHz QPO

By analysing the sidebands of the pulsations we have shown that the pulsed emission couples to the 8 mHz QPO. The fractional modulation of the pulsed emission was found to be systematically lower than that of the direct QPO. Further confirmation that the pulsed emission and the QPO are coupled comes from the detection of a 0.5 coherence measure between them.

Interestingly, the fractional amplitude of the pulse modulation shows the same energy dependence as the direct QPO, with a peak amplitude at 1 keV, and decreasing amplitudes for increasing energy. By contrast, the average pulse amplitude has an opposite energy dependence; the pulse fraction is low at 1 keV and increases steeply over the same energy range (Sanna et al. 2017). Meanwhile, the harmonic of the direct QPO also shows an increasing fractional amplitude with energy. Although the modulation power spectrum does not show a clear harmonic, this trend of an increasing harmonic and decreasing fundamental as a function of energy is also observed in the coherence spectrum.

The pulsations of AMXPs are typically well described by a two component spectral model consisting of a soft thermal blackbody and a hard power-law tail (Gierliński et al. 2002; Poutanen & Gierliński 2003). Both components are associated with the impact of the accretion flow, which is thought to cause a hotspot on the stellar surface and an accretion shock slightly above it. The blackbody is then attributed to the hotspot itself, and the power-law to the accretion shock, which reprocesses the hotspot emission by thermal Comptonization (Gierliński & Poutanen 2005).

The natural explanation for the pulse/QPO coupling would be that the QPO emission originates in the stellar hotspot. This assumption, however, does impose some restrictions on how the pulsed emission arises. If the hotspot emission is modulated by the QPO, then consequently, so are the seed photons that are reprocessed in the accretion shock. However, the pulsed hard power-law emission is apparently not strongly modulated by the QPO, even though the pulse fraction increases with energy. Depending on how the modulation itself arises, two scenarios may be able to explain this observation. First, the QPO may be due to an oscillation in temperature that is localized in certain region of the hotspot (e.g. its edges). In this case the seed photons entering the shock may have a much smaller modulation amplitude than the overall hotspot. Second, the hotspot variability may be due to area variations, so that again the intensity of the seed photons is largely unaffected by the QPO.

As natural consequence of both scenarios the fractional amplitude of pulse modulation should be lower than that of the non-pulsed QPO, as was indeed observed. In the case of temperature oscillations, the ratio of these amplitudes relates to the relative area of the hotspot that is affected by the QPO. For the area variations, on the other hand, this ratio could indicate the size of the area variations, and hence place a limit on the smallest and largest extent of the hotspot. How the opposite energy dependence of the harmonic fits into this picture, however, is not clear.

Any model that aims to explain the QPOs through a variable hotspot should also be able to explain the averaged shape of the pulse profile. We would expect that variations in area and temperature each lead to a slightly different averaged pulse profile, so that detailed modeling of the pulse profile shape as a function of QPO phase could be able to distinguish between the two scenarios. Furthermore, such an approach could potentially break some of the angle degeneracies that exists in pulse profile modeling. Such a detailed pulse profile modeling analysis, however, is beyond the scope of the present work.

5.2. The 20 mHz QPO

The detection of a ~ 20 mHz QPO and its harmonic has been reported for the *RXTE* observations of the 2004 outburst of IGR J00291. A similar mHz QPO has also been reported for the 2008 outburst, although for those observations no harmonic was detected (Hartman et al. 2011).

By analysing the pulse amplitude modulation spectra of these data we have shown that in the 2004 outburst the mHz QPOs are modulating the pulsations. This result demonstrates that the methods introduced in this work can be used to study the coupling of weak aperiodic features with the periodic emission of the pulsar.

We found that the modulation coherence spectra show a series of harmonic peaks with a fundamental frequency of 20 mHz. We note that more harmonic peaks are visible in modulation coherence spectra than are visible in the direct power spectrum. This result suggests that pulse coherent analysis methods, such as discussed here, may be able to extract more intricate information on the driving mechanism than would otherwise be possible.

The identification of these mHz QPOs in the context of variability observed in other LMXBs is uncertain. A possible interpretation is that these features are instances of Low-Frequency (LF) QPOs. In other LMXBs, however, such QPOs show a specific frequency relation with the band-limited noise components. As discussed by Linares et al. (2007), the mHz QPOs in IGR J00291 deviate from that relation by an order of magnitude. Such a deviation may be attributed to the anomalous morphology of the power spectrum (Linares et al. 2007), which has lower characteristic frequencies and larger fractional variability than normally observed.

However, more recently the AMXP MAXI J0911–655 has been shown to exhibit a similar broad noise structure, but with LF QPOs that fall along the expected frequency relation (Bult 2017), casting doubt on this interpretation.

From recent work on black-hole binaries a view has emerged that LF QPOs are due to Lense-Thirring precession of a geometrically thick inner accretion flow that rotates as a solid body (Ingram & van der Klis 2015; Ingram et al. 2016). Extending this model to neutron stars, however, requires additional precession torques due to the stellar oblateness (Morsink & Stella 1999) and magnetic field (Shirakawa & Lai 2002) to be taken into account. The observed deviation from the frequency relation could then be interpreted as evidence that one of these additional effects is dominating the effective precession torque in IGR J00291. In such a model, however, the LF QPO is caused by a geometric effect in the accretion disk. For such a QPO to be coupled to the pulsed emission requires a ‘beating’ interaction model, driven by the stellar magnetosphere or pulsar beam sweeping over the disk. Because this interaction involves two azimuthally rotating components, it should give rise to a single sideband interaction. The mHz QPOs in IGR J00291, however, are observed in both sidebands, which strongly disfavors the precession model as the mechanism behind these QPOs.

Millihertz QPOs have also been observed in a number of atoll sources (Revnivtsev et al. 2001). Their relation with type I X-ray bursts (Altamirano et al. 2008) provides strong evidence these QPOs are somehow related to nuclear burning on the neutron star surface, and are often explained in terms of marginally stable burning (Heger et al. 2007). This model predicts that an oscillation in the thermonuclear burning rate can occur in a narrow range of accretion rates. This interpretation poses a problem for the mHz QPOs of IGR J00291, which are observed throughout the outburst, and thus for a wider range of mass accretion rates than seen in other sources. It is worth pointing out, however, that there are still considerable theoretical uncertainties in the required conditions leading to marginally stable burning. In particular, the mass accretion rates used in simulations differ from those observed by an order of magnitude (Keek et al. 2014). Marginally stable burning therefore remain a possible explanation for the mHz QPOs observed in this source.

Variations in the mass accretion rate offer another class of models that might be responsible for QPOs that couple to the pulsations. In this scenario the variable accretion rate is directly responsible for an oscillation in stellar hotspot emission. In the specific case of IGR J00291, however, an issue is that there are few mechanisms that have sufficiently long timescales to produce mHz variability (see Ferrigno et al. 2017, for a detailed discussion). Our detection of QPO/pulse coupling does not provide further insight. Detailed analysis of the en-

ergy spectra of the direct and modulation QPOs may be able to place additional constraints on such models, however, given limited data quality this was not possible with the available *RXTE* observations.

5.3. Comparing the QPOs

Comparing the coupling characteristics for the *XMM-Newton* mHz QPO with the *RXTE* mHz QPOs gives some clues on whether these phenomena share a common physical mechanism. For one, we note that both QPOs couple to the pulsations, and both appear in symmetrically in the positive and negative sidebands. This alone is already a strong indication that these features are somehow related to emission originating on the stellar surface, and most likely the stellar hotspot.

We also observed a tentative 6 mHz QPO modulating the pulsations in the 2004 outburst, which is not directly visible in the regular power spectrum. If this component is indeed real, it would suggest that whatever mechanism is causing the very soft 8 mHz QPO

in the *XMM-Newton* data, is also active in the 2004 outburst, but at a slightly lower frequency. This interpretation does not imply a relation between the 8 mHz QPO and the 20 mHz QPOs, however, with the striking resemblance between the modulation coherence spectra, especially between the harder *XMM-Newton* band and the *RXTE* observations, a single, non-trivial oscillation of the stellar hotspot seems the most plausible avenue toward explaining all these millihertz features and the characteristics of their coupling with the pulsed emission.

We would like to thank the referee for detailed comments that helped improve the presentation of this work. PB was supported by an NPP fellowship at NASA Goddard Space Flight Center. MvdD and MvdK acknowledge support from the Netherlands Organisation for Scientific Research (NWO).

REFERENCES

- Altamirano, D., van der Klis, M., Wijnands, R., & Cumming, A. 2008, *ApJL*, **673**, L35
- Belloni, T., Psaltis, D., & van der Klis, M. 2002, *ApJ*, **572**, 392
- Bloomfield, P. 1976, *Fourier analysis of time series: an introduction* (New York: Wiley)
- Bracewell, R. 1965, *The Fourier Transform and its applications* (New York: McGraw-Hill)
- Bult, P. 2017, *ApJ*, **837**, 61
- Bult, P., & van der Klis, M. 2014, *ApJ*, **789**, 99
- Burderi, L., Robba, N. R., La Barbera, N., & Guainazzi, M. 1997, *ApJ*, **481**, 943
- Chakrabarty, D., Swank, J. H., Markwardt, C. B., & Smith, E. 2008, *The Astronomer's Telegram*, **1660**, 1
- De Falco, V., Kuiper, L., Bozzo, E., et al. 2017, *A&A*, **599**, A88
- Eckert, D., Walter, R., Kretschmar, P., et al. 2004, *The Astronomer's Telegram*, **352**, 1
- Falanga, M., Kuiper, L., Poutanen, J., et al. 2005, *A&A*, **444**, 15
- Ferrigno, C., Bozzo, E., Sanna, A., et al. 2017, *MNRAS*, **466**, 3450
- Galloway, D. K., Markwardt, C. B., Morgan, E. H., Chakrabarty, D., & Strohmayer, T. E. 2005, *ApJL*, **622**, L45
- Gierliński, M., Done, C., & Barret, D. 2002, *MNRAS*, **331**, 141
- Gierliński, M., & Poutanen, J. 2005, *MNRAS*, **359**, 1261
- Hartman, J. M., Galloway, D. K., & Chakrabarty, D. 2011, *ApJ*, **726**, 26
- Hartman, J. M., Patruno, A., Chakrabarty, D., et al. 2008, *ApJ*, **675**, 1468
- Heger, A., Cumming, A., & Woosley, S. E. 2007, *ApJ*, **665**, 1311
- Ingram, A., & van der Klis, M. 2015, *MNRAS*, **446**, 3516
- Ingram, A., van der Klis, M., Middleton, M., et al. 2016, *MNRAS*, **461**, 1967
- Jenkins, G. M., & Watts, D. G. 1968, *Spectral analysis and its applications* (London: Holden-Day)
- Keek, L., Cyburt, R. H., & Heger, A. 2014, *ApJ*, **787**, 101
- Klein-Wolt, M., Homan, J., & van der Klis, M. 2004, *Nucl. Phys. B*, **132**, 381
- Lazzati, D., & Stella, L. 1997, *ApJ*, **476**, 267
- Leahy, D. A., Darbro, W., Elsner, R. F., et al. 1983, *ApJ*, **266**, 160
- Lewis, F., Linares, M., Russell, D. M., Wijnands, R., & Roche, P. 2008, *The Astronomer's Telegram*, **1726**, 1
- Linares, M., van der Klis, M., & Wijnands, R. 2007, *ApJ*, **660**, 595
- Markwardt, C. B., Swank, J. H., & Strohmayer, T. E. 2004, *The Astronomer's Telegram*, **353**, 1
- Menna, M. T., Burderi, L., Stella, L., Robba, N., & van der Klis, M. 2003, *ApJ*, **589**, 503
- Morsink, S. M., & Stella, L. 1999, *ApJ*, **513**, 827
- Mukherjee, D., Bult, P., van der Klis, M., & Bhattacharya, D. 2015, *MNRAS*, **452**, 3994

- Papitto, A., Bozzo, E., Ferrigno, C., et al. 2011, The Astronomer's Telegram , [3736, 1](#)
- Patruno, A. 2010, [ApJ, 722, 909](#)
- Patruno, A., & Watts, A. L. 2012, ArXiv e-prints , [arXiv:1206.2727 \[astro-ph.HE\]](#), [ads](#)
- Patruno, A., Wijnands, R., & van der Klis, M. 2009, [ApJL, 698, L60](#)
- Poutanen, J., & Gierliński, M. 2003, [MNRAS, 343, 1301](#)
- Revnivtsev, M., Churazov, E., Gilfanov, M., & Sunyaev, R. 2001, [A&A, 372, 138](#)
- Sanna, A., Pintore, F., Bozzo, E., et al. 2017, [MNRAS, 466, 2910](#)
- Shaw, S. E., Mowlavi, N., Rodriguez, J., et al. 2005, [A&A, 432, L13](#)
- Shirakawa, A., & Lai, D. 2002, [ApJ, 564, 361](#)
- Titchmarsh, E. C. 1939, The Theory of Functions (Oxford: Oxford University Press)
- Torres, M. A. P., Jonker, P. G., Steeghs, D., et al. 2008, [ApJ, 672, 1079](#)
- Uttley, P. 2004, [MNRAS, 347, L61](#)
- Uttley, P., & McHardy, I. M. 2001, [MNRAS, 323, L26](#)
- van der Klis, M. 1989, in NATO ASI Series, Vol. 262, Timing Neutron Stars, ed. H. Ögelman & E. P. J. van den Heuvel (Dordrecht: Kluwer), [27](#)
- van der Klis, M. 2006, in Compact stellar X-ray sources, ed. W. H. G. Lewin & M. van der Klis (Cambridge: Cambridge University Press), [39–112](#)
- van Doesburgh, M., & van der Klis, M. 2017, [MNRAS, 465, 3581](#)
- van Straaten, S., van der Klis, M., & Wijnands, R. 2005, [ApJ, 619, 455](#)
- Vaughan, B. A., & Nowak, M. A. 1997, [ApJL, 474, L43](#)
- Zhang, W., Jahoda, K., Swank, J. H., Morgan, E. H., & Giles, A. B. 1995, [ApJ, 449, 930](#)